Competitive effects of nuclear deformation and density dependence of ΛN interaction in B_Λ values of hypernuclei

M. Isaka[1], Y. Yamamoto[2], and Th.A. Rijken[3,2]
[1] *Research Center for Nuclear Physics (RCNP), Osaka University, Ibaraki, Osaka, 567-0047, Japan*
[2] *Nishina Center for Accelerator-Based Science, Institute for Physical and Chemical Research (RIKEN), Wako, Saitama, 351-0198, Japan*
[3] *IMAPP, University of Nijmegen, Nijmegen, The Netherlands*
(Dated: September 21, 2016)

Competitive effects of nuclear deformation and density dependence of ΛN-interaction in Λ binding energies B_Λ of hypernuclei are studied systematically on the basis of the baryon-baryon interaction model ESC including many-body effects. By using the ΛN G-matrix interaction derived from ESC, we perform microscopic calculations of B_Λ in Λ hypernuclei within the framework of the antisymmetrized molecular dynamics under the averaged-density approximation. The calculated values of B_Λ reproduce experimental data within a few hundred keV in the wide mass regions from 9 to 51. It is found that competitive effects of nuclear deformation and density dependence of ΛN-interaction work decisively for fine tuning of B_Λ values.

PACS numbers: Valid PACS appear here

arXiv:1609.06009v1 [nucl-th] 20 Sep 2016

I. INTRODUCTION

Basic quantities in hypernuclei are Λ binding energies B_Λ, from which a potential depth U_Λ in nuclear matter can be evaluated. The early success to reproduce the U_Λ value was achieved by Nijmegen hard-core models [1], where the most important role was played by the ΛN-ΣN coupling term. Medium and heavy Λ hypernuclei have been produced by counter experiments such as (π^+, K^+) reactions. Accurate data of B_Λ values in ground and excited states of hypernuclei have been obtained by γ-ray observations and $(e, e'K^+)$ reactions. With the increase of experimental information [2], precise interaction models have been constructed. In the Nijmegen group, the soft-core models have been developed with continuous efforts so as to reproduce reasonably hypernuclear data [3–6]. In the recent versions of the Extended-Soft Core (ESC) models [5, 6], two-meson and meson-pair exchanges are taken into account explicitly, while these effects are implicitly and roughly described by exchanges of "effective bosons" in one-boson exchange (OBE) models. The latest model ESC08c aims to reproduce consistently almost all features of the $S = -1$ and -2 systems. The parameter fitting has been improved continuously, and the final version has to be submitted soon. In Ref. [9], they used successfully the version of 2012 in the early stage of parameter fitting [7], denoted as ESC08c(2012) [1]. This version is used also in the present work.

Recently, the dependence of B_Λ on structures of core nuclei, in particular nuclear deformations, has been discussed in p shell [8], and *sd-pf* shell hypernuclei [9–11] theoretically. Generally, values of B_Λ are related to nuclear structure in two ways: One is that an increase of deformation reduces the overlap of the densities between a Λ particle and the core nucleus, which makes B_Λ smaller. Such effects are seen in *sd-pf* shell hypernuclei. In Refs. [9, 11], the antisymmetrized molecular dynamics for hypernuclei (HyperAMD) [12, 13] was applied to several *sd-pf* shell hypernuclei such as ${}^{41}_{\Lambda}$Ca and ${}^{46}_{\Lambda}$Sc. It is found that B_Λ values in deformed states are decreased reflecting smaller overlaps.

The other effect is due to the density dependence of the ΛN effective interaction. In light hypernuclei and/or dilute states like cluster states, the density overlap between a Λ and nucleons is significantly decreased, which can affect the B_Λ through the density dependence. For example, in Be hypernuclei having a 2α cluster structure with surrounding neutrons, it was discussed that the overlap becomes much smaller in the well-pronounced 2α cluster states [8]. When the ΛN effective interaction derived from the G-matrix calculation is designed to depend on the nuclear Fermi momentum k_F, the smaller overlap makes the relevant value of k_F small, *i.e.* less Pauli-blocking, resulting in the increase of B_Λ. Considering this effect, it is expected that appropriate values of k_F in finite systems are reduced as overlaps become small with mass numbers, which would affect the mass dependence of B_Λ.

ΛN interactions are related intimately to the recent topic of heavy neutron stars (NS). The stiff equation of state (EoS) giving the large NS-mass necessitates the strong three-nucleon repulsion in the high-density region, the existence of which has been established by many works [14] in nuclear physics. However, the hyperon mixing in neutron-star matter brings about the remarkable softening of the EoS, canceling this repulsive effect. A possible way to solve such a problem is to assume that strong repulsions exist universally in three-baryon channels. More specifically, it is assumed that the ΛNN repulsion works in Λ hypernuclei as well as the three-nucleon repulsion. A ΛNN three-body effect, that is

[1] The fortran code ESC08c2012.f is put on the permanent open-access website, NN-Online facility: *http://nn-online.org*.

generally a hyperonic many-body effect (MBE), has to appear as an additional density dependence of the ΛN effective interaction. It is important to study MBE by analyzing the experimental data of B_Λ systematically.

The aim of the present work is to reveal how the density dependence of the ΛN effective interaction affects the mass dependence of B_Λ. Since the *p-sd-pf* shell hypernuclei have various structures in the ground states, they would affect the values of B_Λ through the density-dependence of the ΛN interaction. To investigate it, we use the HyperAMD combined with ΛN *G*-matrix interaction, which successfully describes various structures of hypernuclei without assumptions on specific clustering and deformations [12, 13].

This paper is organized as follows. In the next section, the ΛN G-matrix interaction is explained as well as treatment of MBE. In Sec. III, we explain how to describe hypernuclei, namely the theoretical framework of HyperAMD. In Sec. IV, we show the calculated values of B_Λ including MBE, and discuss effects from core structures on B_Λ . Section V summarizes this paper.

II. ΛN G-MATRIX INTERACTION

We start from ESC08c(2012), which was used in the analysis of Λ hypernuclei based on the HyperAMD most successfully [9]. One should be careful, however, that the main conclusion in this work has to be valid qualitatively also for other realistic interaction models including ΛN-ΣN coupling terms which lead to strong density dependences of the ΛN effective interactions. Hereafter, ESC08c(2012) is denoted as ESC simply. As a model including an additional density dependence due to a hyperonic MBE, we adopt the model given in Ref. [15]. Here, the multi-pomeron exchange repulsion (MPP) is added into ESC together with the phenomenological three-body attraction (TBA), where both of them are represented as density-dependent two-body interactions. Using ESC+MPP+TBA, G-matrix calculations are performed with the continuous choice for off-shell single particle potentials: Contributions of MPP and TBA are renormalized into ΛN G-matrices. The MPP part is given as

$$V^{(N)}_{MPP}(r;\rho) = g^{(N)}_P g^N_P \frac{\rho^{N-2}}{\mathcal{M}^{3N-4}} \left(\frac{m_P}{\sqrt{2\pi}}\right)^3 \exp\left(-\frac{1}{2}m_P^2 r^2\right), \quad (1)$$

corresponding to triple ($N = 3$) and quartic ($N = 4$) pomeron exchange. The values of the two-body pomeron strength g_P and the pomeron mass m_P are the same as those in ESC. A scale mass $\mathcal{M}$ is taken as the proton mass. The TBA part is assumed as

$$V_{TBA}(r;\rho) = V_0 \exp(-(r/2.0)^2)\, \rho \exp(-3.5\rho)\, (1+P_r)/2 \ , \quad (2)$$

P_r being a space-exchange operator. In Refs. [15, 16], these interactions were assumed to be universal in all baryonic channels. Namely, the parameters $g^{(3)}_P$, $g^{(4)}_P$ and V_0 in hyperonic channels were taken to be the same as those in nucleon channels, assuring the stiff EoS of hyperon-mixed neutron-star matter. There were used three sets with different strengths of MPP in Refs. [15, 16]. In the case of the set MPa, for instance, the parameters were taken as $g^{(3)}_P = 2.34$, $g^{(4)}_P = 30.0$ and $V_0 = -32.8$. In the present analysis, however, such a choice leads to a too strong density-dependence of the ΛN G-matrix interaction for reproducing the mass dependence of B_Λ values: In the case of ESC08c(2012), the mass dependence of B_Λ values are reproduced rather well without the additional MBE. Then, the values of $g^{(3)}_P$ and $g^{(4)}_P$ may be much smaller than the above values so that the additional density dependence is not strong. Here, the parameters are determined so that calculated results of B_Λ values in the present framework are consistent with the experimental data. They are taken as $g^{(3)}_P = 0.39$, $g^{(4)}_P = 0.0$ and $V_0 = -5.0$: MPP (TBA) is far less repulsive (attractive) than those in the above case. In this case, the calculated value of B_Λ is 13.0 MeV in ${}^{16}_{\Lambda}$O, which is consistent with the observed value (see Table III). Thus, MBE is represented by MPP+TBA, having only minor effects on the results in this work.

TABLE I: Values of parameters in $\Delta V_{\Lambda N}(k_F;r) = (a+bk_F+ck_F^2)\exp-(r/\beta_2)^2$ with $\beta_2 = 0.9$ fm.

	${}^1E$	${}^3E$	${}^1O$	${}^3O$
a	4.809	4.345	2.701	1.611
b	−11.09	−10.57	−7.743	−5.704
c	5.264	5.035	8.004	7.599

ΛN G-matrix interactions $V_{\Lambda N}$ for ESC are constructed in nuclear matter with Fermi momentum k_F [17]. They are represented in coordinate space and parameterized in a three-range Gaussian form [17],

$$V_{\Lambda N}(r;k_F) = \sum_{i=1}^{3} (a_i + b_i k_F + c_i k_F^2) \exp\left(-r^2/\beta_i^2\right) \ . \quad (3)$$

The parameters (a_i, b_i, c_i) are determined so as to simulate the calculated G-matrix for each spin-parity state. The procedures to fit the parameters are given in Ref. [17], and the determined parameters for ESC are given in Ref. [9].

Contributions from MBE (MPP+TBA) to G-matrices are represented by modifying the second-range parts of $V_{\Lambda N}(k_F, r)$ for ESC by $\Delta V_{\Lambda N}(k_F, r) = (a + bk_F + ck_F^2)\exp\left\{-(r/\beta_2)^2\right\}$. It should be noted that the values of parameters $g^{(3)}_P$, $g^{(4)}_P$ and V_0 are connected to the values of a, b and c through this procedure. The values of parameters are given in Table I.

In applications of nuclear matter G-matrix interactions $V_{\Lambda N}(r;k_F)$ to finite systems, a basic problem is how to

TABLE II: Values of B_Λ in ${}^{89}_{\Lambda}$Y and ${}^{16}_{\Lambda}$O calculated with ADA and LDA (in MeV). Observed values of B_Λ ($B_\Lambda^{\rm exp}$) are shifted by 0.54 MeV from those in Refs. [18, 19] as explained in Sec. IV A.

	$-B_\Lambda^{\rm cal}$		
	ADA	LDA	$-B_\Lambda^{\rm exp}$
${}^{89}_{\Lambda}$Y	-23.7	-23.6	-23.65 ± 0.10 [18]
${}^{16}_{\Lambda}$O	-13.3	-12.3	-12.96 ± 0.05 [19]

choose k_F values in each system: An established manner is to use so called local-density and averaged-density approximations *etc* based on physical insight. As the better choice to describe Λ single particle (s.p.) states, we adopt an averaged-density approximation (ADA) [17], where the averaged value of k_F is defined by

$$k_F = \left(\frac{3\pi^2\langle\rho\rangle}{2}\right)^{1/3}, \langle\rho\rangle = \int d^3r \rho_N(\mathbf{r})\rho_\Lambda(\mathbf{r}). \quad (4)$$

In the case of local-density approximation (LDA), k_F values are obtained from $(\rho_N(\mathbf{r}) + \rho_\Lambda(\mathbf{r}))/2$ as a function of $\mathbf{r}$. We compare ADA and LDA by calculating B_Λ values for ${}^{89}_{\Lambda}$Y and ${}^{16}_{\Lambda}$O with use of the Λ-nucleus folding model in which ΛN G-matrix interactions $V_{\Lambda N}(r; k_F)$ are folded into density distributions [17]. For spherical-core systems, the results calculated with the G-matrix folding model are similar to those with the HyperAMD used in the following section. In Table II, the result is shown in the case of using ESC without MBE. It is demonstrated here that the B_Λ values in ${}^{89}_{\Lambda}$Y are reproduced nicely in both cases of ADA and LDA with no adjustable parameter. On the other hand, in ${}^{16}_{\Lambda}$O, the value of B_Λ obtained with LDA is found to be smaller than that with ADA. Thus, the B_Λ values with LDA are similar to (smaller than) those with ADA in heavy (light) systems, and eventually the mass dependence of B_Λ values can be reproduced better using ADA than LDA. Hence, the ADA is employed in the present work as an approximate way to use nuclear matter G-matrix interactions in finite systems.

III. ANALYSIS BASED ON HYPERAMD

In this study, we apply the HyperAMD to p, sd, and pf shell Λ hypernuclei, namely from ${}^{9}_{\Lambda}$Li up to ${}^{59}_{\Lambda}$Fe, in order to describe various structures of these hypernuclei such as an α clustering and prolate, oblate, and triaxial deformations in ground states. Combined with the generator coordinate method (GCM), we perform the systematic analysis of B_Λ.

A. Hamiltonian and wave function

The Hamiltonian used in this study is

$$H = T_N + T_\Lambda - T_g + V_{NN} + V_C + V_{\Lambda N}, \quad (5)$$

where T_N, T_Λ, and T_g are the kinetic energies of the nucleons, Λ particle, and center-of-mass motion, respectively. We use Gogny D1S [20, 21] as the effective nucleon-nucleon interaction V_{NN}, and the Coulomb interaction V_C is approximated by the sum of seven Gaussians. As for the ΛN interaction $V_{\Lambda N}$, we use the G-matrix interaction discussed above.

The variational wave function of a single Λ hypernucleus is described by the parity-projected wave function, $\Psi^\pm = \hat{P}^\pm\{\mathcal{A}\{\varphi_1, \ldots, \varphi_A\} \otimes \varphi_\Lambda\}$, where

$$\varphi_i \propto e^{-\sum_\sigma \nu_\sigma \left(r_\sigma - Z_{i\sigma}\right)^2} \otimes (u_i\chi_\uparrow + v_i\chi_\downarrow) \otimes (p \text{ or } n), \quad (6)$$

$$\varphi_\Lambda \propto \sum_{m=1}^{M} c_m e^{-\sum_\sigma \nu_\sigma \left(r_\sigma - z_{m\sigma}\right)^2} \otimes (a_m\chi_\uparrow + b_m\chi_\downarrow). \quad (7)$$

Here the s.p. wave packet of a nucleon φ_i is described by a single Gaussian, while that of Λ, φ_Λ, is represented by a superposition of Gaussian wave packets. The variational parameters are $\boldsymbol{Z}_i$, $\boldsymbol{z}_m$, ν_σ, u_i, v_i, a_m, b_m, and c_m. In the actual calculation, the energy variation is performed under the constraint on the nuclear quadrupole deformation parameters (β, γ) in the same way as in Ref. [13]. By the frictional cooling method, the variational parameters in $\Psi^\pm$ are determined for each set of (β, γ), and the resulting wave functions are denoted as $\Psi^\pm(\beta, \gamma)$.

B. Angular momentum projection and generator coordinate method

After the variation, we project out the eigenstate of the total angular momentum J for each set of (β, γ) (angular momentum projection; AMP),

$$\Psi^{J\pm}_{MK}(\beta, \gamma) = \frac{2J+1}{8\pi^2} \int d\Omega D^{J*}_{MK}(\Omega) R(\Omega) \Psi^\pm(\beta, \gamma). \quad (8)$$

The integrals over the three Euler angles Ω are performed numerically. Then the wave functions with differing values of K and (β, γ) are superposed (generator coordinate method; GCM):

$$\Psi^{J\pm}_n = \sum_p \sum_{K=-J}^{J} c_{npK} \Psi^{J\pm}_{MK}(\beta_p, \gamma_p). \quad (9)$$

The coefficients c_{npK} are determined by solving the Griffin-Hill-Wheeler equation [13].

C. B_Λ and analysis of wave function

The B_Λ's are calculated as the energy difference between the ground states of a hypernucleus $({}^{A+1}_{\Lambda}Z)$

TABLE III: $-B_\Lambda$ [MeV] calculated with ESC + MBE together with $\langle\rho\rangle$ [fm^{-3}] and k_F [fm^{-1}] defined by Eq.(4), and nuclear quadrupole deformation (β,γ) for each hypernucleus. Values in parentheses are calculated with ESC08c(2012) only in unit of MeV. Observed values $B_\Lambda^{\rm exp}$ are taken from Refs. [2, 18, 19, 22–28]. Values of $B_\Lambda^{\rm exp}$ with dagger are also explained in text.

	β	γ	$\langle\rho\rangle$	k_F	$-B_\Lambda^{\rm cal}$	$-B_\Lambda^{\rm exp}$
${}^{9}_{\Lambda}$Li	0.50	2°	0.072	1.02	−8.1(−7.9)	-8.50 ± 0.12[24]
${}^{9}_{\Lambda}$Be	0.87	1°	0.060	0.96	−8.1(−7.9)	-6.71 ± 0.04[25]
${}^{9}_{\Lambda}$B	0.45	2°	0.072	1.02	−8.2(−8.0)	-8.29 ± 0.18[24]
${}^{10}_{\Lambda}$Be	0.57	1°	0.077	1.04	−9.0(−8.7)	-9.11 ± 0.22[23], -8.55 ± 0.18[28]
${}^{10}_{\Lambda}$B	0.68	1°	0.075	1.04	−9.2(−8.9)	-8.89 ± 0.12[25]
${}^{11}_{\Lambda}$B	0.50	29°	0.081	1.05	−10.1(−9.8)	-10.24 ± 0.05[25]
${}^{12}_{\Lambda}$B	0.39	44°	0.083	1.07	−11.3(−11.0)	-11.37 ± 0.06[25], -11.38 ± 0.02[27]
${}^{12}_{\Lambda}$C	0.41	34°	0.086	1.08	−11.0(−10.7)	-10.76 ± 0.19[24]
${}^{13}_{\Lambda}$C	0.45	60°	0.090	1.10	−11.6(−11.3)	-11.69 ± 0.19[23]
${}^{14}_{\Lambda}$C	0.52	22°	0.093	1.11	−12.5(−12.4)	-12.17 ± 0.33[24]
${}^{15}_{\Lambda}$N	0.28	60°	0.098	1.13	−12.9(−12.6)	-13.59 ± 0.15[25]
${}^{16}_{\Lambda}$O	0.02	–	0.105	1.16	−13.0(−12.7)	-12.96 ± 0.05[19]†
${}^{19}_{\Lambda}$O	0.30	3°	0.110	1.18	−14.3(−14.0)	–
${}^{21}_{\Lambda}$Ne	0.46	0°	0.106	1.16	−15.4(−15.1)	–
${}^{25}_{\Lambda}$Mg	0.478	21°	0.116	1.20	−16.1(−15.8)	–
${}^{27}_{\Lambda}$Mg	0.36	36°	0.125	1.23	−16.3(−16.4)	–
${}^{28}_{\Lambda}$Si	0.32	53°	0.125	1.23	−16.6(−16.4)	-17.1 ± 0.02[2]†
${}^{32}_{\Lambda}$S	0.23	16°	0.130	1.24	−17.6(−17.4)	-18.0 ± 0.5[22]†
${}^{40}_{\Lambda}$K	0.01	–	0.136	1.26	−19.4(−19.2)	–
${}^{40}_{\Lambda}$Ca	0.03	–	0.136	1.26	−19.4(−19.2)	-19.24 ± 1.1[26]†
${}^{41}_{\Lambda}$Ca	0.13	12°	0.136	1.26	−19.6(−19.4)	–
${}^{48}_{\Lambda}$K	0.01	–	0.141	1.27	−20.2(−20.1)	–
${}^{51}_{\Lambda}$V	0.18	2°	0.151	1.31	−20.4(−20.4)	-20.51 ± 0.13[18]†
${}^{59}_{\Lambda}$Fe	0.26	23°	0.142	1.28	−21.4(−21.3)	–

and the core nucleus $({}^AZ)$ as $B_\Lambda = E({}^AZ;j^\pm) - E({}^{A+1}_{\Lambda}Z;J^\pm)$, where $E({}^AZ;j^\pm)$ and $E({}^{A+1}_{\Lambda}Z;J^\pm)$ are calculated by GCM.

We also calculate squared overlap between the $\Psi^{J\pm}_{MK}(\beta,\gamma)$ and GCM wave function $\Psi^{J\pm}_{\alpha}$,

$$O^{J\pm}_{MK\alpha}(\beta,\gamma) = |\langle\Psi^{J\pm}_{MK}(\beta,\gamma)|\Psi^{J\pm}_{\alpha}\rangle|^2, \qquad (10)$$

which we call the GCM overlap. $O^{J\pm}_{MK\alpha}(\beta,\gamma)$ shows the contribution of $\Psi^{J\pm}_{MK}(\beta,\gamma)$ to each state $J^\pm$, which is useful to estimate deformation of each state. In this study, we regard (β,γ) corresponding to the maximum value of the GCM overlap as nuclear deformation of each state.

IV. RESULTS AND DISCUSSIONS

A. B_Λ in p,sd, and pf shell Λ hypernuclei

The calculated values of B_Λ for ESC including MBE are summarized in Table III together with the values of k_F and $\langle\rho\rangle$, and compared with those calculated by using ESC only (in parentheses) and observed values of B_Λ ($B_\Lambda^{\rm exp}$). Here, the k_F values are calculated by Eq.(4) on the basis of ADA. In Table III, we also show (β,γ) which gives the maximum value of the GCM overlap defined by Eq.(10). Recently, in Ref. [28], it has been discussed that the $B_\Lambda^{\rm exp}$ measured by the (π^+,K^+) experiments are systematically shallower by 0.54 MeV in average than the emulsion data for ${}^{7}_{\Lambda}$Li, ${}^{9}_{\Lambda}$Be, ${}^{10}_{\Lambda}$B and ${}^{13}_{\Lambda}$C. It indicates that the reported binding energy of ${}^{12}_{\Lambda}$C [24] would be shallower by 0.54 MeV, which is used for the binding energy measurements as the reference in the (π^+,K^+) experiments. Therefore, in Table III, the values of $B_\Lambda^{\rm exp}$ measured by the (π^+,K^+) or (K^-,π^-) experiments (with dagger) are shifted by 0.54 MeV deeper from the values reported by Refs. [2, 18, 19, 22, 26]. In spite of this correction, there still remain calibration ambiguities in the (π^+,K^+) data. One should be careful for this problem, when the calculated values of B_Λ are compared with these data.

Let us discuss the calculated values of B_Λ shown in Table III. As mentioned in Sec. II, we determine the parameters of MPP and TBA in Eqs. (1) and (2) so as to reproduce $B_\Lambda^{\rm exp}$ in ${}^{16}_{\Lambda}$O in the HyperAMD calculation with ESC + MPP + TBA. It is seen that the B_Λ with ESC + MPP + TBA reproduces the observed data within about 200 keV except for ${}^{9}_{\Lambda}$Be, ${}^{15}_{\Lambda}$N and ${}^{28}_{\Lambda}$Si, which is achieved owing to the k_F dependence of the ΛN G-matrix interaction used. As seen in Table III, the k_F values become small with decreasing mass number, which means that the ΛN G-matrix interaction becomes attractive. The main origin of the k_F dependence is from the ΛN-ΣN coupling terms included in ESC.

B. Effects of core deformation

For the fine agreement of B_Λ values to the experimental data, it is very important to describe properly the core structures, in particular nuclear deformations. Recently, many authors have been studying deformations of hypernuclei in p-shell [29–32], sd-shell [9, 10, 29–34], and pf-shell [9, 10, 29] mass regions. In this study, we take into account deformations of hypernuclei by performing GCM calculations in which intrinsic wave functions with various (β,γ) deformations $\Psi^\pm(\beta,\gamma)$ are diagonalized.

In order to study the importance of core deformations in the systematic calculations of B_Λ values, we perform the GCM calculation by using the spherical wave functions $\Psi^{J\pm}_{MK}(\beta=0.0)$ in Eq.(9) (case (B)), whereas Table III summarizes the GCM results with various deformations (case (A)). In the case (B), the k_F value is determined independently from the case (A) with $\Psi^{J\pm}_{MK}(\beta=0.0)$ by Eq.(4) for each hypernucleus. By using the k_F values determined in the case (B), we also perform the GCM calculations with various (β,γ) deformations (case (C)). Table IV shows the calculated values of B_Λ in the cases (A) - (C) in the typical p-shell hypernuclei ${}^{11}_{\Lambda}$B, ${}^{12}_{\Lambda}$B, and ${}^{13}_{\Lambda}$C. Comparing the cases (A) and (B), we find the considerable discrepancy of B_Λ, *i.e.* the B_Λ in the

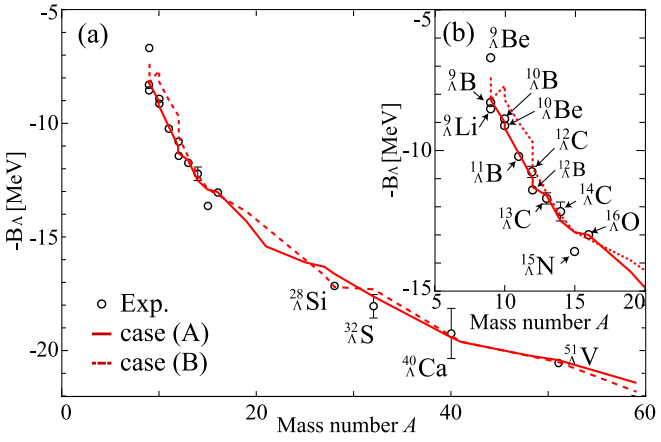

FIG. 1: (Color online) (a) Comparison of B_Λ between cases (A) (solid) and (B) (dashed). Open circles show observed values with mass numbers from $A = 9$ up to $A = 51$, which are taken from Refs. [2, 18, 19, 22–27]. $B_\Lambda^{\rm exp}$ measured by (π^+, K^+) and (K^-, π^-) reactions are shifted by 0.54 MeV as explained in text. (b) Same as (a), but magnified in the $5 \le A \le 20$ region.

case (B) are shallower than those in the case (A), which indicates that the B_Λ becomes smaller, if the core nuclei are spherical. This is mainly due to the larger k_F value in the case (B) compared with the case (A), which comes from the increase of $\langle\rho\rangle$ in a spherical state (see Eq.(4)). For example, in the case of $^{12}_{\Lambda}$B, the obtained value of B_Λ is 9.7 MeV with $k_F = 1.16$ fm^{-1} in the case (B), whereas $B_\Lambda = 11.3$ MeV with $k_F = 1.07$ fm^{-1} in the case (A) (*cf.* $B_\Lambda^{\rm exp} = 11.4 \pm 0.02$ MeV [27]). The same difference between the cases (A) and (B) is seen in the other hypernuclei, in particular light hypernuclei with $A < 16$, as shown in Figure 1 (a) and (b).

In Table IV, it is also found that the values of B_Λ in the case (C) are shallower than those in the case (B), which deviate much from those in the case (A) and the observations. This is because the deformation of the core nuclei decreases the overlap between the Λ and core nuclei. Since we use the same k_F in the cases (B) and (C), the smaller overlap with deformation in the case (C) makes B_Λ shallower. Therefore, it can be said that the consistent descriptions of the deformation and the values of k_F determined in deformed states are essential to reproduce the observations. B_Λ values are given by the balance of two competitive effects: (1) The deformation makes the Λ s.p. energy (k_F value) shallower (smaller). (2) The smaller value of k_F makes the Λ s.p. energy deeper due to the density dependence of ΛN interaction. In $A > 16$ region, generally, deformations make B_Λ values smaller because the effect (2) is not so remarkable to cancel the effect (1). On the other hand, in $A < 16$ region, deformations make B_Λ values larger due to the effect (2).

Let us confirm whether the core deformation is successfully described under the present AMD framework with the Gogny D1S interaction. It can be done essentially by comparing $E2$ transition probabilities $B(E2)$ of the core nuclei with the observations, which are quite sensitive to the nuclear deformation. For example, in $^{12}_{\Lambda}$B, we calculate $B(E2)$ in ^{11}B as $B(E2; 5/2^-_1 \to 3/2^-_1) = 16\ e^2\text{fm}^4$ by performing the GCM calculation with various (β, γ) deformations following Refs. [35, 36], which is consistent with the experimental value $B(E2; 5/2^-_1 \to 3/2^-_1) = 14 \pm 3\ e^2\text{fm}^4$ [37]. On the basis of the structure calculation for ^{11}B, we obtain a very reasonable value of B_Λ in $^{12}_{\Lambda}$B by the addition of a Λ particle. Then, it is confirmed that our calculations for B_Λ are performed in the model space to describe core deformations properly.

Here, we compare the deformation of hypernuclei with that predicted by Ref. [30], in which $^{13}_{\Lambda}$C and $^{28}_{\Lambda}$Si are predicted to be spherical within the framework of relativistic mean-field, whereas the core nuclei ^{12}C and ^{27}Si are oblately deformed. It means that the addition of a Λ particle makes the core nucleus spherical. In the present work, we also find the reduction of the core deformation by the addition of a Λ particle. However, the degree of deformation change is rather small. Thus these hypernuclei are still deformed as shown in Table III, while $(\beta, \gamma) = (0.50, 59^\circ)$ in ^{12}C and $(\beta, \gamma) = (0.35, 55^\circ)$ in ^{27}Si. This difference between the present work and Ref. [30] mainly comes from the effects by rotational motions, which are included by performing the angular momentum projection (AMP) (see Eq.(8)). In fact, it is also found that the deformation of $^{13}_{\Lambda}$C becomes spherical before performing the AMP [32], which is the same trend as predicted by Ref. [30]. In the present calculation, not only rotational motions but also configuration mixing and shape fluctuations are taken into account by performing the AMP and GCM, which can affect the deformation of hypernuclei.

C. Deviation of B_Λ in several hypernuclei

We comment on the large deviation of B_Λ in $^{9}_{\Lambda}$Be, $^{15}_{\Lambda}$N, and $^{28}_{\Lambda}$Si. In $^{9}_{\Lambda}$Be, it is considered that the Gogny D1S force [20, 21] overestimates the size of each α particle of 2α cluster structure of the core ^{8}Be due to the zero-range density-dependent term, as pointed out by Ref. [38], which would cause the overestimation of B_Λ by the decrease of k_F through Eq.(4). It is found that the k_F value which reproduces the $B_\Lambda^{\rm exp}$ of $^{9}_{\Lambda}$Be ($k_F = 1.08$ fm^{-1}) is much larger than that shown in Table III ($k_F = 0.96$ fm^{-1}). The smallness of the latter value of k_F is due to the overestimation of the size of α with Gogny D1S. It is also found that the same phenomenon appears in the Λ hypernuclei with $A < 9$ having α cluster structure by using Gogny D1S. Therefore, we exclude them from being the subject of the present analysis. In such cases, it would be necessary to use appropriate effective NN interactions instead of Gogny D1S. In $^{15}_{\Lambda}$N, the $B_\Lambda^{\rm exp}$ measured by the emulsion experiment [25] seems to be deviating from those of the neighboring hypernuclei in Figure 1(b). This might be due to the difficulties of the analysis

TABLE IV: Comparison of B_Λ with the cases (A), (B) and (C) in ${}^{11}_{\Lambda}$B, ${}^{12}_{\Lambda}$B, and ${}^{13}_{\Lambda}$C. Value of k_F calculated by Eq.(4) in each case is also shown. (β, γ) giving the maximum values of the GCM overlap (Eq.(10)) are also shown in cases (A) and (C).

	${}^{11}_{\Lambda}$B			${}^{12}_{\Lambda}$B			${}^{13}_{\Lambda}$C		
	case (A)	case (B)	case (C)	case (A)	case (B)	case (C)	case (A)	case (B)	case (C)
$-B_\Lambda$	-10.1	-9.0	-8.7	-11.3	-9.7	-9.4	-11.6	-11.5	-10.5
k_F	1.05	1.13	1.13	1.07	1.16	1.16	1.10	1.15	1.15
(β, γ)	(0.50,29°)		(0.50,29°)	(0.39,44°)		(0.39,44°)	(0.45,60°)		(0.45,60°)
$-B_\Lambda^{\rm exp}$	-10.24 ± 0.05[25]			-11.37 ± 0.06[25],-11.38 ± 0.02[27]			-11.69 ± 0.19[23]		

and smaller numbers of events in the emulsion experiments. Therefore, we hope to perform a new analysis of the emulsion measurements with large statistic in the future. In ${}^{28}_{\Lambda}$Si, the value of B_Λ is underestimated in case (A), whereas that in case (B) (17.3 MeV) is much closer to the experimental value. This might be due to an overestimation of the core deformation, which is seen in the comparison of the electric quadrupole moment Q in the ground state $5/2^+$ of ^{27}Si, namely, $Q(5/2^+, \mathrm{AMD}) = 10$ e fm^2, whereas $Q(5/2^+, \exp) = 6.1 \pm 0.4$ e fm^2 [39]. Since the calculated values of k_F are almost the same in the cases (A) and (B) (1.23 fm^{-1}), the value of B_Λ would be in between the values of these cases, if the deformation of ^{27}Si is smaller than the present result.

D. B_Λ and strength of many-body force

Finally, we also comment on the relation between B_Λ and the strength of MPP and TBA. In the present study, the parameters $g_P^{(3)}$ and $g_P^{(4)}$ in Eq.(1) (V_0 in Eq.(2)) are taken as far smaller (less attractive) than those in in Refs. [15, 16]. They are determined so as to improve the fitting of B_Λ values to the experimental data. As seen in Table III, the calculated values of B_Λ with ESC only reproduce rather well the experimental ones. Therefore, there remains only a small room to introduce MBE on the basis of ESC. On the other hand, in case of MPa [15, 16], the parameters of MPP and TBA in hyperonic channels are taken to be the same as those in nucleon channels assuming the stiff EoS of hyperon mixed neutron-star matter. It is found that values of B_Λ are overestimated if the parameter set of MPa is used combined with ESC. For example, B_Λ with MPa are 13.0 MeV for ${}^{13}_{\Lambda}$C (*cf.* $B_\Lambda^{\rm exp} = 11.69 \pm 0.19$ MeV), and 14.2 MeV for ${}^{16}_{\Lambda}$O (*cf.* $B_\Lambda^{\rm exp} = 12.96 \pm 0.05$ MeV). This indicates that the strength of MPP and TBA in MPa is too strong to reproduce the observations, when MPa is used together with ESC. It is known that two-body ΛN effective interactions still have ambiguities, and thus potential depth and k_F dependence are different among models. The dependence of MBE on two-body ΛN effective interaction models will be discussed in following paper. Here, for instance, the strong MPP such as MPa is shown to be allowable in the case of the latest version of ESC08c.

V. SUMMARY

On the basis of the baryon-baryon interaction model ESC including MBE, competitive effects of nuclear deformation and density dependence of the ΛN interaction are investigated. By using the G-matrix interaction derived from ESC, we perform microscopic calculations of B_Λ within the framework of HyperAMD with the ADA treatment for the hypernuclei with $9 \leq A \leq 59$. It is found that the calculated values of B_Λ reproduce the experimental data within a few hundred keV, when the additional density dependence by MBE is taken into account. This is achieved by the competition between the nuclear deformation and density dependence of ΛN interaction. Generally, the overlap between the Λ and nucleons varies depending on the degree of core deformation. In the light hypernuclei with $A \leq 16$, it is found that the B_Λ becomes larger by the density dependence of the ΛN interaction, because the overlap rapidly decreases for increasing deformation, which mainly comes from the ΛN-ΣN coupling. On the other hand, in *sd-pf* shell hypernuclei, the change of the overlap is rather small even if the core deformation is enhanced. Therefore, the density dependence does not affect the B_Λ significantly. Instead, increasing deformation makes B_Λ smaller by decreasing the overlap. Thus, both of taking into account the core deformations and the treatment of the density dependence of the ΛN interaction are essential to understand the systematic behavior of B_Λ.

[1] M.M.Nagels, T.A.Rijken and J.J.deSwart, Phys. Rev. **D15** (1977), 2547; **D20** (1979), 1633.

[2] O. Hashimoto and H. Tamura, Prog. Part. and Nucl. Phys. **57**, (2006) 564.

[3] P.M.M.Maessen, T.A.Rijken, and J.J.deSwart, Phys. Rev. **C40** (1989), 2226.

[4] Th.A. Rijken, V.G.J. Stoks, and Y. Yamamoto, Phys. Rev. **C59** (1999), 21.

[5] Th.A.Rijken and Y.Yamamoto, Phys. Rev. **C73** (2006), 044008.

[6] Th.A. Rijken, M.M. Nagels, and Y. Yamamoto, Prog. Theor. Phys. Suppl. **185**, 14 (2010).

[7] Th.A. Rijken, M.M. Nagels, and Y. Yamamoto, in *Proceedings of the International Workshop on Strangeness*

Nuclear Physics, Neyagawa 2012, Genshikaku Kenkyu **57**, Suppl.3, 6 (2013).
[8] M. Isaka and M. Kimura, Phys. Rev. C**92**, 044326(2015)
[9] M. Isaka, K. Fukukawa, M. Kimura, E. Hiyama, H. Sagawa, and Y. Yamamoto, Phys. Rev. C**89**, (2014) 024310.
[10] B.-N. Lu, E. Hiyama, H. Sagawa, and S.-G. Zhou, Phys. Rev. C**89**, 044307 (2014).
[11] M. Isaka, M. Kimura, E. Hiyama, and H. Sagawa, Prog. Theor. Exp. Phys. **103** D02(2015).
[12] M. Isaka, M. Kimura, A. Dote, and A. Ohnishi, Phys. Rev. C**83**, (2011) 054304.
[13] M. Isaka, H. Homma, M. Kimura, A. Dote, and A. Ohnishi, Phys. Rev. C**85**, (2012) 034303.
[14] For example, S.C. Pieper, V.R. Pandharipande, R.B. Wiringa, and J. Carlson, Phys. Rev. C**64**, (2001) 014001.
[15] Y.Yamamoto, T.Furumoto, N.Yasutake and Th.A.Rijken, Phys. Rev. C**90**, (2014) 045805.
[16] Y.Yamamoto, T.Furumoto, N.Yasutake and Th.A.Rijken, Phys. Rev. C**88**, (2013) 022801.
[17] Y.Yamamoto, T.Motoba, Th.A. Rijken, Prog. Theor. Phys. Suppl. **No.185** (2010), 72.
[18] H. Hotchi *a*l., Phys. Rev. C**64**, (2001) 044302.
[19] S. Ajimura *e*t. *a*l., Nucl. Phys. A**639**, (1998) 93c.
[20] J. Decharge and D. Gogny, Phys. Rev. C**21** (1980) 1568.
[21] J.F. Berger, M. Girod and D. Gogny, Comp. Phys. Comm.**63** (1991) 365.
[22] R. Bertini *a*l., Nucl. Phys. A**83**, (1979) 306.
[23] D.H. Davis, Nucl. Phys. A**547**, (1992) 369.
[24] D.H. Davis, Nucl. Phys. A**754**, (2005) 3c.
[25] M. Jurič *a*l., Nucl. Phys. B**52**, (1973) 1.
[26] P.H. Pile *a*l., Phys. Rev. Lett. **66**, (1991) 2585.
[27] L. Tang, *e*t. *a*l., Phys. Rev. C**90**, (2014) 034320.
[28] T. Gogami *et al.*, Phys. Rev. **C93** (2016), 034314.
[29] Xian-Rong Zhou, H.-J. Schulze, H. Sagawa, Chen-Xu Wu, and En-Guang Zhao, Phys. Rev. C**76**, (2007) 034312.
[30] M.T. Win and K. Hagino, Phys. Rev. C**78**, (2008) 054311.
[31] Bing-Nan Lu, En-Guang Zhao, and Shan-Gui Zhou, Phys. Rev. C**84**, (2011) 014328.
[32] M. Isaka, M. Kimura, A. Doté and A. Ohnishi, Phys. Rev. C**83**, (2011) 044323.
[33] H.-J. Schulze, M. T. Win, K. Hagino, and H. Sagawa, Prog. Theor. Phys.**123**, (2010) 569.
[34] J. M. Yao, Z. P. Li, K. Hagino, M. T. Win, Y. Zhang, and J. Meng, Nucl. Phys. A**868**, (2011) 12.
[35] T. Suhara and Y. Kanada-En'yo, Prog. Theor. Phys. **123**, (2010) 303.
[36] T. Suhara and Y. Kanada-En'yo, Phys. Rev. C**85**, (2012) 054320.
[37] Ajzenberg-Selove, Nuc. Phys. A**506**, (1990) 1.
[38] Y. Kanada-En'yo and Y. Akaishi, Phys. Rev. C**69**, (2004) 034306.
[39] N. Stone, At. Data Nucl. Data Tables **90**, 75 (2005).